

Structural transformations in morphotropic-phase-boundary composition of the lead-free piezoelectric system $\text{Ba}(\text{Ti}_{0.8}\text{Zr}_{0.2})\text{O}_3 - (\text{Ba}_{0.7}\text{Ca}_{0.3})\text{TiO}_3$

Kumar Brajesh, Muluaem Abebe, and Rajeev Ranjan*

Department of Materials Engineering, Indian Institute of Science, Bangalore 560012, India

(Received 19 June 2016; published 9 September 2016)

The exceptionally large piezoelectric response of the morphotropic-phase-boundary (MPB) composition of the lead-free piezoelectric system $(1-x)\text{Ba}(\text{Ti}_{0.8}\text{Zr}_{0.2})\text{O}_3 - x(\text{Ba}_{0.7}\text{Ca}_{0.3})\text{TiO}_3$ has attracted great attention in recent years. Here in this paper we report a detailed investigation of the structural phase transformation behavior of the MPB composition ($x = 0.50$) driven by electric field, stress, and temperature. We show that the system exhibits metastable phases in a wide temperature range, and that the large piezoresponse at room temperature has a significant contribution from the increased fraction of the metastable phases induced by the poling field. Using a “powder poling” technique we also demonstrate the equivalence of stress and electric field with regard to the nature of the structural transformation. The fundamental significance of this interesting observation is discussed.

DOI: [10.1103/PhysRevB.94.104108](https://doi.org/10.1103/PhysRevB.94.104108)

I. INTRODUCTION

Due to the toxicity of lead in the commercially used lead zirconate titanate (PZT) based piezoelectric materials, there is an increasing emphasis on lead-free piezoelectrics exhibiting a large piezoelectric response. In this context, the BaTiO_3 based piezoelectric alloy system $(1-x)\text{Ba}(\text{Ti}_{0.8}\text{Zr}_{0.2})\text{O}_3 - x(\text{Ba}_{0.7}\text{Ca}_{0.3})\text{TiO}_3$ (BCTZ) has attracted considerable attention in the recent past because of its exceptionally large piezoelectric properties (e.g., $d_{33} \sim 600$ pC/N) [1–7]. The highest piezoresponse in this alloy system has been reported for the morphotropic-phase-boundary (MPB) composition $x = 0.50$. The understanding of the mechanism associated with the extraordinary piezoelectric response is still far from complete, one of the important reasons being the lack of clarity with regard to the subtleties of the structure(s) and phase transition behavior. Liu and Ren [1] associated the large piezoresponse to the system’s proximity to a cubic-tetragonal-rhombohedral triple point. Keeble *et al.*, on the other hand, attributed it to a “convergence region” in the phase diagram where tetragonal ($P4mm$), orthorhombic ($Amm2$), and rhombohedral ($R3m$) phases approach each other [4]. Experiments, however, suggest that large piezoelectric response occurs in the vicinity of the tetragonal-orthorhombic phase boundary instead of the convergence region [8]. A similar observation has also been reported in Zr, Sn, and Hf substituted BaTiO_3 [9–11] although the piezoelectric response of these systems is comparatively less than in BCTZ. There is a lack of unanimity with regard to the crystallographic state of the MPB composition close to room temperature (~ 25 °C). Using convergent beam electron diffraction (CBED) technique Gao *et al.* reported a coexistence of $P4mm$ and $R3m$ phases [12]. Other groups have reported an orthorhombic ($Amm2$) phase in the immediate vicinity of the tetragonal phase [4,13,14]. This was countered by Gao *et al.* [5] who argued that the $Amm2$ phase observed in the x-ray diffraction patterns is most likely due to adaptive diffraction by rhombohedral/tetragonal nanodomains. Haugen *et al.* also concluded in favor of the $P4mm + R3m$ phase

coexistence model by Rietveld analysis of high-resolution x-ray diffraction data [3]. A coexistence of three phases, $P4mm + Amm2 + R3m$, was recently reported by Brajesh *et al.* [7].

Alongside the ongoing debate with regard to the crystallographic state of the MPB composition, attempts have also been made to understand the structural/microstructural mechanisms associated with the large piezoresponse of this system using electric-field-dependent x-ray diffraction studies [8,14,15]. Tutuncu *et al.* have focused on the tetragonal ($P4mm$) rich compositions and established a correlation between enhanced non-180° domain wall motion and reduced tetragonality near the MPB [15]. A dominant contribution of the ferroelastic domain wall motion in determining the piezoresponse was also highlighted in tetragonal compositions close to the MPB by Ehmke *et al.* [16]. Based on analogy with other lead-based MPB systems such as $\text{Pb}(\text{Zr},\text{Ti})\text{O}_3$ [17] and $\text{PbTiO}_3 - \text{BiScO}_3$ [18], Brajesh *et al.* have argued that field induced tetragonal to orthorhombic/rhombohedral transformation could be the most important factor regarding the large piezoresponse of the MPB compositions of the BCTZ. Since the piezoelectric phenomenon is described in two ways, namely, (i) direct piezoelectric effect, wherein the stimulus is the stress and the measured response is the change in polarization, and (ii) converse piezoelectric effect wherein the electric field is the stimulus and the response is strain, it is of also of fundamental interest to compare the nature of the phase transformation induced by stress and electric field separately in piezoceramics. Presumably due to experimental convenience, electric field has been the most commonly used stimulus to study the structural/microstructural cause-effect relationships in piezoceramics. The role of stress has not received serious attention so far in the literature. In this paper, we report a comparative study of the role of stress and electric field with regard to the nature of phase transformation in this interesting piezoelectric system. We show that irrespective of the nature of the stimulus (electric field or stress) the piezoceramic shows the same phase transformation behavior. We have also carried out a detailed structural study as a function of temperature and show that the system exhibits metastable phases in a wide temperature range. Our study suggests that the increased

*rajeev@materials.iisc.ernet.in

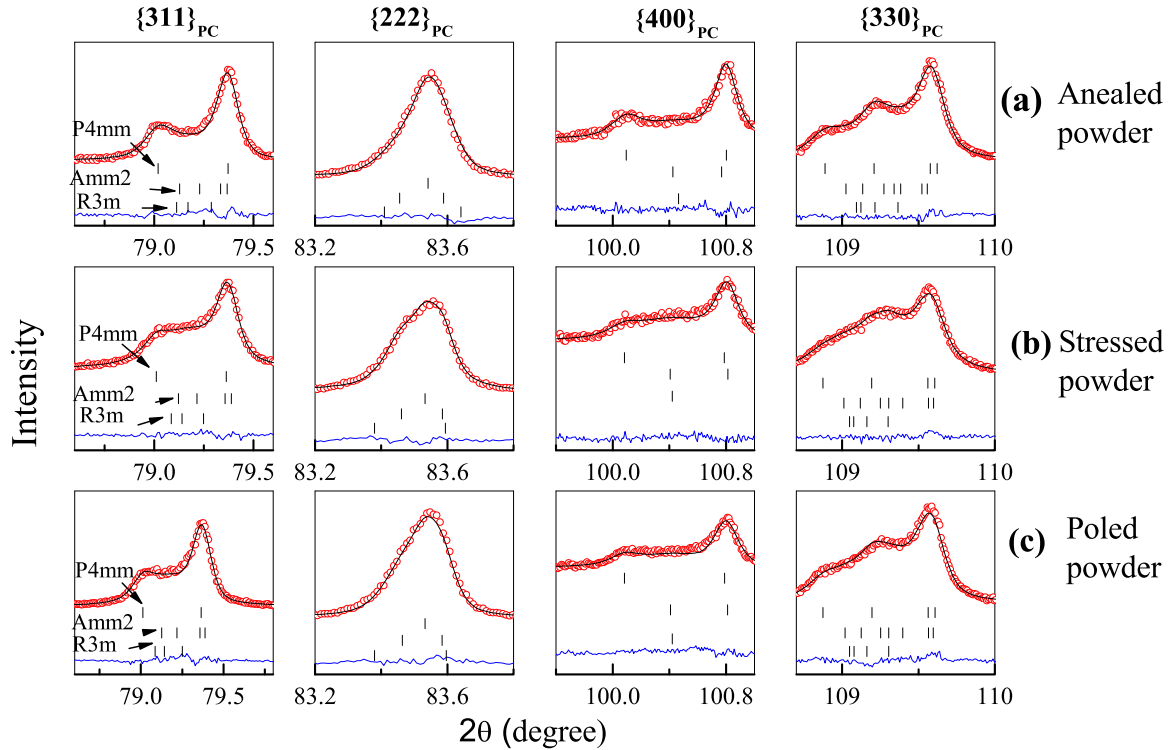


FIG. 1. Rietveld fitted x-ray powder diffraction profiles of representative high-angle pseudocubic reflections of (a) annealed specimen, (b) stressed specimen, and (c) poled powder specimen.

fraction of the metastable phases by poling plays an important role in significantly enhancing the piezoelectric response of this system.

II. EXPERIMENT

The MPB composition $0.5\text{Ba}(\text{Ti}_{0.8}\text{Zr}_{0.2})\text{O}_3 - 0.5(\text{Ba}_{0.7}\text{Ca}_{0.3})\text{TiO}_3$ also referred to as $(\text{Ba}_{0.85}\text{Ca}_{0.15})(\text{Ti}_{0.90}\text{Zr}_{0.10})\text{O}_3$ (or BCTZ 15/10 in brief) was prepared via the conventional solid-state route. High-purity BaCO_3 (99.8%; Alfa Aesar), CaCO_3 (99.99%; Alfa Aesar), TiO_2 (99.8%; Alfa Aesar), and ZrO_2 were thoroughly mixed in a zirconia jar using zirconia balls and acetone as the mixing medium via a planetary ball mill (Fritsch P5). The thoroughly mixed powder was calcined at 1300°C for 4 h and milled again in acetone for 5 h for better homogenization. We may note that the milling process did not contaminate the calcined powder as there was no evidence of zirconia peaks in the x-ray diffraction (XRD) patterns of the milled calcined powder. The particle size of the calcined powder was ~ 70 nm. The calcined powder was mixed with 2 wt. % polyvinyl alcohol (PVA) and pressed into disks of 15 mm diameter by using uniaxial dry pressing at 10 ton. Sintering of the pellets was carried out at 1550°C for 2 h under ambient condition. X-ray powder diffraction was done using a Rigaku SmartLab with a Johansson monochromator in the incident beam to remove the $\text{Cu-K}\alpha_2$ radiation. Dielectric measurement was carried out using a Novocontrol (Alpha-A) impedance analyzer. Measurement of the longitudinal piezoelectric coefficient (d_{33}) was carried using piezotest PM 300 by poling the pellets at room temperature for 1 h at a field of ~ 2.2 kV/mm. Strain

loop and polarization electric-field hysteresis loop were measured with a Precision Premier II loop tracer. Structure refinement was carried out using FULLPROF software [19].

III. RESULTS

A. Stress- and electric-field-driven transformation

Figure 1 compares the $\{222\}_{\text{pc}}$ and $\{400\}_{\text{pc}}$ pseudocubic x-ray Bragg profiles of 15/10 BCTZ of an annealed powder specimen [Fig. 1(a)] and also after having subjected it to a uniaxial stress of ~ 300 MPa [Fig. 1(b)]. Since the annealed specimen represents the equilibrium state, the significant change in the profile shape after application of pressure suggests a stress induced phase transformation. Since in our experiment we have recorded the changes not while the stress was applied, but only after its removal, the change in the structure suggests a lack of complete reversibility of the stress induced transformation. We carried out Rietveld analysis to ascertain the nature of the phase transformation. In the previous study, we have shown that the equilibrium state of the MPB composition is characterized by the coexistence of three phases— $P4mm + Amm2 + R3m$ with tetragonal $P4mm$ as the dominant phase [7]. Accordingly, Rietveld analysis was carried out with the three-phase model for the stressed powder. The excellent quality of the fit to the observed pattern with this model is evident from Fig. 1. The refined structural parameters are listed in Table I. The volume fractions of the $P4mm : Amm2 : R3m$, as obtained from the Rietveld analysis of the XRD pattern of the stressed specimen, were found to be 32:51:17. A part of the stressed powder was annealed at 400°C , well beyond the Curie point (95°C), to

TABLE I. Refined structural parameters and agreement factors for the stressed $(\text{Ba}_{0.85}\text{Ca}_{0.15})(\text{Ti}_{0.9}\text{Zr}_{0.1})\text{O}_3$.

Atoms	Space group: $P4mm$				Space group: $Amm2$				Space group: $R3m$			
	X	y	z	$B (\text{\AA}^2)$	x	y	z	$B (\text{\AA}^2)$	x	y	Z	$B (\text{\AA}^2)$
Ba/Ca	0.000	0.000	0.000	0.16(3)	0.00	0.000	0.000	0.17(1)	0.000	0.000	0.000	0.76(6)
Ti/Zr	0.500	0.500	0.524(3)	0.18(6)	0.500	0.000	0.487(4)	0.20(4)	0.000	0.000	0.477(2)	0.17(1)
O1	0.500	0.500	0.036(9)	0.19(3)	0.000	0.000	0.574(8)	0.1(0)	0.312(0)	0.181(0)	0.653(5)	0.1(0)
O2	0.500	0.000	0.52(1)	0.25(2)	0.500	0.255(2)	0.288(6)	0.08(0)				
$a = 3.9991(4) \text{\AA}$, $c = 4.0195(1) \text{\AA}$				$a = 3.9984(3) \text{\AA}$, $b = 5.6764(1) \text{\AA}$,				$a = 5.6751(1) \text{\AA}$, $c = 6.9342(6) \text{\AA}$				
$v = 64.283(1) \text{\AA}^3$, % phase = 32(2)				$c = 5.6661(2) \text{\AA}$, $v = 128.601(3) \text{\AA}^3$,				$v = 193.41(2) \text{\AA}^3$, %phase = 17(3)				
				%phase = 51(2)								
$R_p : 9.48, R_{wp} : 9.70, R_{exp} : 7.56, \chi^2 : 1.64$												

get rid of the stress induced ferroelastic changes. Rietveld analysis of this annealed specimen gave a volume fraction of the $P4mm : Amm2 : R3m$ ratio as 56:32:12. This establishes a stress induced $P4mm \rightarrow Amm2 + R3m$ transformation in this system.

To compare the nature of the stress-driven transformation with that of the transformation induced by electric field, we adopted a “powder poling technique” [20–22]. This strategy was adopted to avoid the preferred orientation effect inevitably shown by pellet specimens when subjected to electric field (due to the ferroelectric-ferroelastic domain reorientation with field). Preferred orientation diffraction data are not desirable for reliable structural analysis, more so when the specimen comprises different phases with nearly similar pseudocubic lattice parameters. Although the preferred orientation effect in a poled pellet can be nullified by breaking the pellet into small particles, the stress applied to the specimen during the grinding process would have its own effect. The structural change observed in such a powder should in principle be attributed to both the electric field and stress imposed during the grinding process. To get rid of the grinding process, it was necessary to develop a technique wherein the annealed powder particles are directly subjected to electric field.

The key to our strategy involves embedding the powder particles in a polymeric matrix and subjecting the polymer-ceramic composite to a high electric field. The powder is then retrieved by dissolving the polymeric matrix. The technique involves the following steps: (i) A sintered pellet is first ground to obtain the powder. (ii) This powder is then annealed well above the Curie point to eliminate the stress induced ferroelastic changes, if any, brought about during the grinding process. (iii) The annealed powder is gently and thoroughly mixed with 1–2 wt. % of acryl polymer powder for about 15–20 min and the ceramic-polymer mixture is compacted in the form of a green pellet. (iv) The compact was gently wetted by drop-by-drop soaking with a companion liquid acryl solvent and subsequently cured for ~ 24 h. After curing the composite pellet became a dense solid. (v) The dense compact was heated at 200°C for ~ 1 h to relieve the stress induced changes before the application of the poling field. In a separate experiment we verified that the x-ray powder diffraction pattern of the powder retrieved after annealing the composite at 200°C for 1 h was identical to that of the annealed powder used for making the composite itself. This ensured that the very formation

of the composite itself did not introduce any feature of its own. The dense compact was poled at high field ~ 40 kV/cm, much above the coercive field (~ 3 kV/cm). After poling the polymer part of the composite was dissolved in acetone and the ceramic powder retrieved. The powder thus obtained is termed as “poled powder.” Because it is a powder specimen, the use of this poled powder would give a preferred orientation free diffraction pattern, which is desirable for reliable structural analysis, more so in situations as in the present case where three phases are coexisting. The poled powder is expected to carry the information about the nature of phase transformation the crystallites would have undergone while the field was on. It may be noted that in case a field induced phase transformation is completely reversible, this strategy would be irrelevant. From the x-ray powder diffraction of the poled powder of BCTZ 15/10, shown in Fig. 1(c), it is evident that the shape of the $\{222\}_{pc}$ profile is similar to the shape of this profile when the crystallites were subjected to pure stress. Similarly, there is a noticeable enhancement in the intensity between the 004 and 400 tetragonal peaks as compared to the annealed specimen. The similarity of the XRD patterns of the specimen subjected to stress and that subjected to electric field confirms that both the stimuli induce exactly the same phase transformation in the MPB composition of BCTZ.

B. Temperature-driven structural transformations

Figure 2 shows the temperature dependence of the dielectric behavior of BCTZ 15/10 from -100°C to $+200^\circ\text{C}$. Three dielectric anomalies at $\sim 90^\circ\text{C}$, $\sim 30^\circ\text{C}$, and $\sim 0^\circ\text{C}$ can be noticed in this plot. The dielectric peak near 90°C is representative of tetragonal-cubic, ferroelectric-paraelectric transformation. As will be shown below, the two low-temperature dielectric anomalies at $\sim 30^\circ\text{C}$ and 0°C are associated with the $P4mm$ - $Amm2$ and $Amm2$ - $R3m$ transitions, respectively. An interesting point to note in the dielectric plot is the onset of dielectric dispersion below 200°C and its persistence down to the $P4mm$ - $Amm2$ transition. The significance of this will be discussed later. Figure 3 shows the x-ray powder diffraction profiles of a few selected pseudocubic Bragg reflections on cooling below room temperature. A noticeable change can be seen in the profile shapes when the temperature is reduced from 30°C to 20°C . For example, a hump develops on the left of the main peak in $\{222\}_{pc}$ and additional featureless intensity appears between the two tetragonal peaks in $\{400\}_{pc}$.

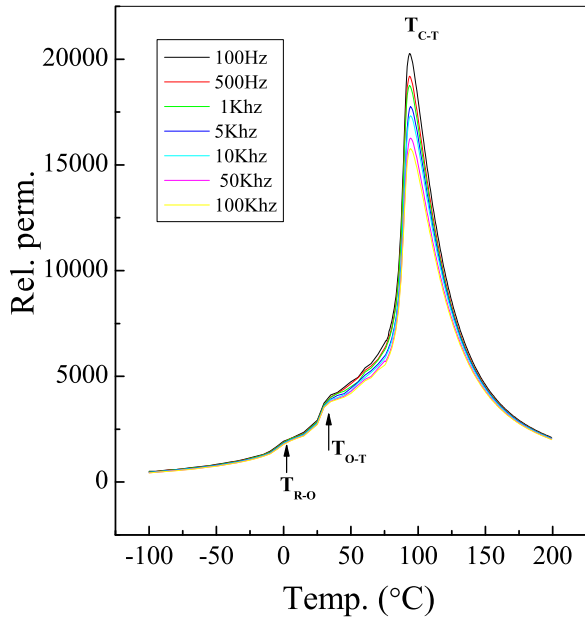


FIG. 2. Temperature dependence of the relative permittivity of BCTZ 15/10 at different frequencies. The arrows highlight the transitions.

This temperature is close to the dielectric anomaly at $\sim 30^\circ\text{C}$ in Fig. 2. The system appears to completely transform to the $Amm2$ phase at 10°C . On further cooling, the next transformation is evident below 0°C . For example, while at 0°C the two peaks in the $\{200\}_{pc}$ profile are nearly equal in intensity; at -25°C , the height of the peak on the right is significantly reduced at 0°C . Similarly, a considerable reduction in the intensity of the left peak in the $\{222\}_{pc}$ doublet can be seen at -25°C . The structural transition is therefore consistent with the dielectric anomaly at $\sim 0^\circ\text{C}$, Fig. 2. The $Amm2$ - $R3m$ transformation, however, seems to be very sluggish since the rhombohedral phase, which is characterized by a singlet $\{400\}_{pc}$ and a doublet $\{222\}_{pc}$, can be seen only below -25°C , for example at -50°C , Fig. 3. From the visual inspection of the $\{400\}_{pc}$ profile at 0°C and -25°C , it is evident that the majority phase at -25°C is still orthorhombic. Figure 4 shows the Rietveld analysis of XRD patterns for two temperatures 10°C and -100°C , the visual inspection of which suggests orthorhombic and rhombohedral phases, respectively. The overall fit of the 10°C pattern appears reasonably good with a pure orthorhombic structural model, Fig. 4(a). However, subtle misfit regions, as indicated by arrows in the magnified pseudocubic $\{222\}_{pc}$ profile, suggest the need to consider a second phase. The inclusion of the $R3m$ phase in the structural analysis takes care of every detail of the $\{222\}_{pc}$ profile, as shown in Fig. 4(b). A comparison of the two fits suggests that with the single-phase $Amm2$ model, the software attempts to obtain the best fit by increasing the width of the Bragg profiles. This way it tries to compensate for the additional intensities due to another phase, not accounted for in the model. The improved fit of the pseudocubic $\{222\}_{pc}$ profile with addition of the $R3m$ structure is due to the fact that the $R3m$ phase predicts a Bragg peak near the tail of the $\{222\}_{pc}$ on the left side, and also another peak adjacent to the Bragg

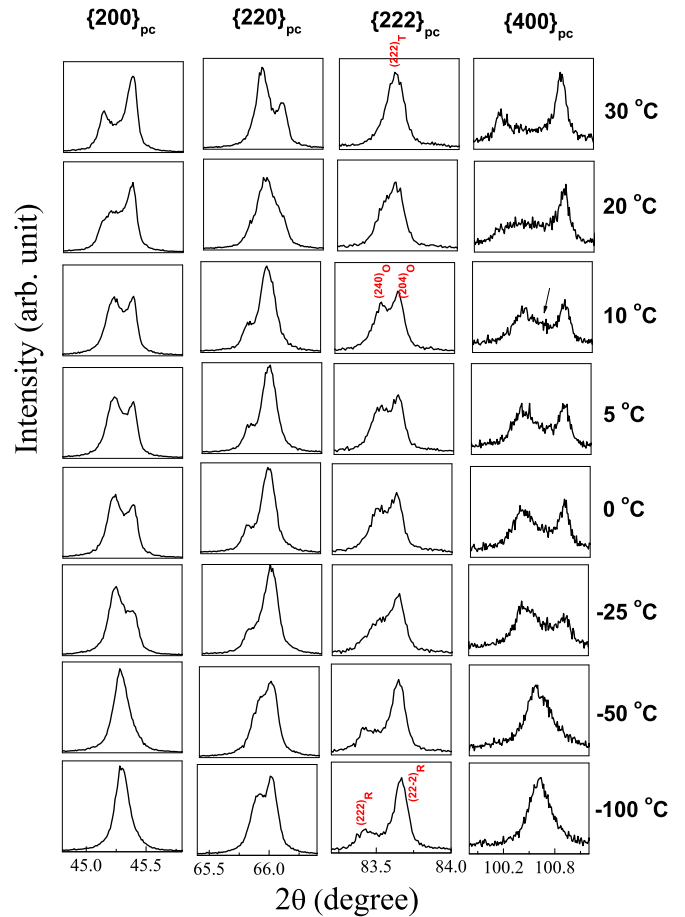


FIG. 3. Evolution of the pseudocubic profiles of BCTZ 15/10 as a function of temperature. The arrow indicates asymmetry in the profile at a position which matches with the Bragg peak corresponding to the $R3m$ phase. The Miller indices of the distinct peaks in the pseudocubic $\{222\}_{pc}$ profile are shown. The subscripts T, O, and R in the Miller indices denote the tetragonal, orthorhombic, and the rhombohedral phases.

peak of the $Amm2$ phase on the right side. Moreover, a clear asymmetry on the right side of the left peak in $\{400\}_{pc}$ at 10°C (Fig. 3) is also an indicator of the presence of an additional peak corresponding to the $R3m$ phase, since the $Amm2$ structural model predicts only two Bragg peaks for this pseudocubic profile. Although from visual inspection the doublet nature of the pseudocubic $\{222\}_{pc}$ and the singlet nature of the pseudocubic $\{400\}_{pc}$ suggest a $R3m$ structure at -50°C and -100°C , Fig. 3, Rietveld analysis revealed a very poor fit of the $\{222\}_{pc}$ with the single-phase $R3m$ model, Fig 4(c). A dramatic improvement in the fit takes place by including the orthorhombic ($Amm2$) phase, Fig. 4(d). Our structural analysis suggests that the ferroelectric state of BCTZ 15/10 comprises metastable phases in a wide temperature range.

IV. DISCUSSION

A. Nature of the phase coexistence

Apart from the convergent beam electron diffraction study of Gao *et al.* which suggests the presence of $R3m$ symmetry near room temperature of the MPB composition of BCTZ,

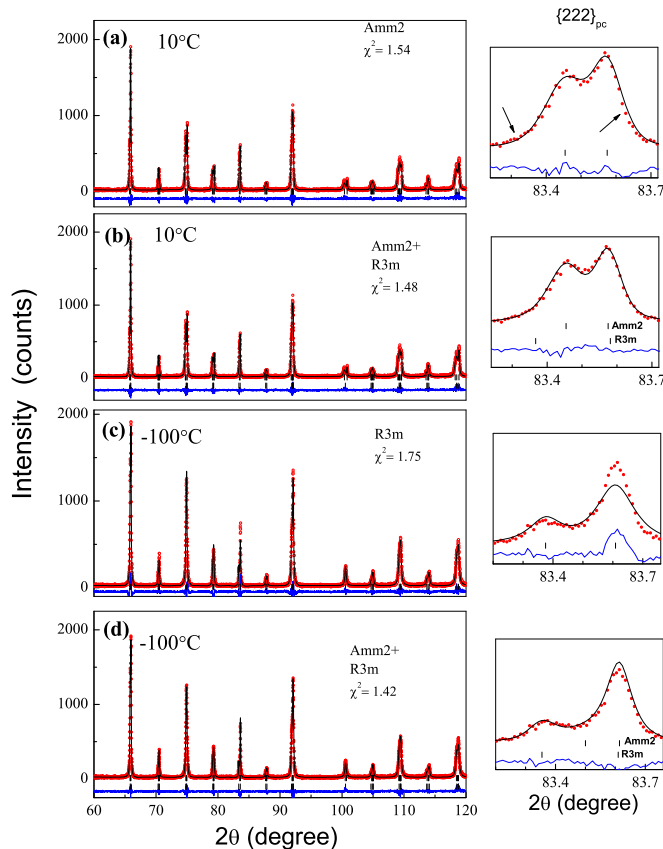


FIG. 4. Rietveld fitted x-ray powder diffraction pattern of BCTZ 15/10 at 10 °C and –100 °C with two different structural models. The fitting of the pseudocubic $\{222\}_{pc}$ profile with the different models is highlighted in the magnified plot in the figures on the right.

the lack of unanimity with regard to the structural state, even among groups dealing with the interpretation of the x-ray diffraction data, seems to arise due to nearly similar pseudocubic lattice parameters of the $Amm2$ and $R3m$ phases. This aspect can be easily seen in the analysis of Haugen *et al.* who argued that the best fit was obtained with a $P4mm + R3m$ phase coexistence model. A careful perusal of the fit at 20 °C shown by Haugen *et al.* [3] using the $P4mm + R3m$ phase coexistence model reveals that the fitted profile of the pseudocubic $\{222\}_{pc}$ does not exactly pass through the observed data points. Our study suggests that the crucial information with regard to the structural distortions is contained in the shape of the $\{222\}_{pc}$ and the $\{400\}_{pc}$ pseudocubic profiles. For the $P4mm$ structure the $\{222\}_{pc}$ is a singlet. It is a doublet with nearly equal intensity for $Amm2$. These doublets appear in the immediate proximity on either side of the tetragonal $(222)_T$ peak, as is evident from the evolution of the $Amm2$ phase, Fig. 3. With respect to the $Amm2$ cell the two orthorhombic peaks have the indices $(240)_O$ and $(204)_O$. The $R3m$ distortion also splits the $\{222\}_{pc}$ into two with rhombohedral Miller indices being $(222)_R$ for the peak on the left and $(22-2)_R$ for the peak on the right, Fig. 3. It is important to recognize that the rhombohedral $(22-2)_R$ and the orthorhombic peak $(204)_O$ both appear on the right side of the tetragonal $(222)_T$ and overlap severely. The rhombohedral $(222)_R$ appears at a noticeably lower 2θ position

than the orthorhombic $(240)_O$ peak, which our diffractometer can easily resolve. In our analysis we have used the distinct nonoverlapping peaks $(222)_R$ and $(240)_O$ as the guide to ascertain the presence of $R3m$ and $Amm2$ phases, respectively, in BCTZ. The structural analysis using the Rietveld method was accordingly carried out. This strategy gave consistent results and very good fits of the observed diffraction pattern for all the different diffraction patterns (stress, electric field, temperature dependent). The inability of the $P4mm + R3m$ model to fit the observed $\{222\}_{pc}$ profile precisely in Ref. [3] can be understood from the fact that the $R3m$ Bragg peaks try to account for the peaks which are, in principle, due to the $Amm2$ phase. The fact that the attempt by the authors to include the $Amm2$ phase resulted in an unstable refinement [3] can be attributed to the fact that both $Amm2$ and $R3m$ phases are competing to fit the same features in the diffraction profiles. In the absence of a significant number of distinct peaks characteristic of the coexisting phases, Rietveld analysis is incapable of achieving the right set of lattice parameters for the different phases, leading to oscillatory refinement, as reported in Ref. [3]. A similar situation has been reported in other ferroelectric systems exhibiting multiple phases with very similar pseudocubic lattice parameters [23–25]. In our case, the oscillatory refinement could be avoided because right in the beginning of the refinement, nearly accurate lattice parameters of the coexistence phases were used to account for the characteristic peaks of the $Amm2$ and the $R3m$ phases, mentioned above. Although similar to Keeble *et al.* [4] we obtained a reasonably good average fit of the diffraction pattern at 10 °C with a single-phase $Amm2$ model, the fact that a noticeable misfit occurs in the $\{222\}_{pc}$ profile with pure $Amm2$ phase, and not so after inclusion of the $R3m$ phase, proves the continuity of the $R3m$ phase in the $Amm2$ stability region. The continuity of the $R3m$ as a metastable phase should be expected in the temperature region corresponding to a stable $Amm2$ phase since its existence as a metastable phase has already been shown at ~ 25 °C. Our findings seem to rationalize the electron diffraction studies of Gao *et al.* showing evidence of $R3m$ symmetry in the vicinity of room temperature [5], and also of Keeble *et al.* suggesting $Amm2$ phase [4]. It is interesting to note that the $Amm2$ continues to exist as a metastable phase deep in the $R3m$ stability region. This perhaps is indicative of the very sluggish nature of this transformation. One possible reason for this sluggishness could be the kinetic barriers associated with the preexisting ferroelastic-ferroelectric domains (and the domain walls) of the high-temperature phases—the formation of the $R3m$ phase along with its domain configuration has to take place within the already existing complex orthorhombic domains, which in turn have grown in preexisting tetragonal domains. The existence of both $Amm2$ and $R3m$ as metastable phases near 25 °C could be an important factor for the exceptionally large piezoelectric response of the MPB composition of BCTZ. An interesting result in support of this argument comes from the slight increase in the maximum value of the dielectric anomaly associated with the $Amm2$ - $P4mm$ transition temperature in the poled specimen as compared to the unpoled specimen, Fig 5. In an experiment we carried out heating and cooling dielectric measurements on a poled specimen in a limited temperature range 30°–50° (i.e., well below the

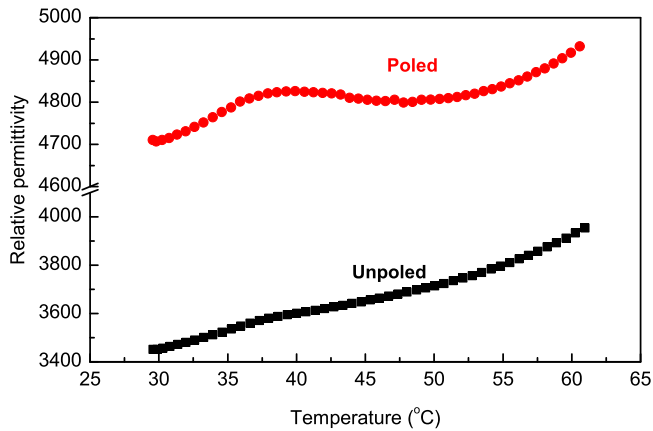


FIG. 5. Temperature dependence of relative permittivity in a limited temperature range of unpoled and poled pellet of BCTZ 15/10. The same pellet was used for the two measurements to avoid a possible specimen to specimen variation of the permittivity.

tetragonal-cubic transition temperature). The distinct dielectric peak at $\sim 35^\circ\text{C}$ was suppressed in the cooling cycle. The d_{33} value after this cooling decreased by $\sim 130\text{ pC/N}$ (from 570 to 440 pC/N). This seems to suggest that a significant contribution to the weak-field direct piezoelectric response is associated with the field stabilized metastable phase(s). Stabilization of $Amm2$ as a metastable phase after poling has also been reported in pure BaTiO_3 thereby suggesting that this tendency is present even in the parent compound [22].

B. Decrease in the polarization coherence after poling

Apart from the distinct anomaly associated with the $Amm2$ - $P4mm$ transformation clearly evident in the poled specimen, Fig. 5 also shows that the permittivity of the poled specimen is significantly enhanced after poling. This could be related to the increased structural (and hence polar) heterogeneity in the poled specimen because of the increased fraction of the metastable phases. In this interpretation we assume that with a decrease in the correlation length of polarization, the polar relaxation will increase and would lead to enhancement in the permittivity. This aspect is very well known in relaxor ferroelectrics [26]. However, contrary to our case, application of strong field in the nonergodic state of a relaxor ferroelectric increases the coherence length of polarization and thereby decreases permittivity [26]. The increase in permittivity after poling in our case can be attributed to increase in the structural heterogeneity by field induced $P4mm$ to $Amm2 + R3m$ transformation. Another plausible explanation of the enhanced permittivity after poling could be associated with the anisotropy of the dielectric constant in the various phases, and increased fraction of the domain variants with higher dielectric constant in the direction of the field after poling. Contrary to the previous explanation, this is a purely structural argument. Another notable observation is the significant dielectric dispersion in the temperature range $+200^\circ\text{C}$ down to 30°C , Fig. 2. The onset of the frequency dispersion below $\sim 200^\circ\text{C}$ is indicative of the development of polar nanoregions in the cubic matrix as in the relaxor ferroelectric systems [26].

From this viewpoint, the dielectric maximum at $\sim 92^\circ\text{C}$ is associated with a relaxor to normal ferroelectric transformation on cooling. Unlike in the lead-based relaxor ferroelectrics wherein the positional disorder of Pb ion plays a predominantly important role in the relaxor state, the relaxor ferroelectric state in a BaTiO_3 based system, such as $\text{Ba}(\text{Ti},\text{Zr})\text{O}_3$, is due to the difference in the ferroelectric strengths of the Ti^{4+} and Zr^{4+} ions [27–29]. This difference in the off centering of Zr and Ti ions gives rise to Fano resonance and thermally activated THz relaxation [29]. Petzelt *et al.* have reported that the Ti^{4+} dynamics does not freeze completely in the nonergodic state of $\text{Ba}(\text{Ti}_{1-x}\text{Zr}_x)\text{O}_3$ [30–32]. The persistence of the dielectric dispersion below the dielectric maximum down to 30°C , i.e., until the $P4mm$ - $Amm2$ transformation, however, suggests that the tetragonal ferroelectric regions are still small in size. The significantly reduced tetragonality of this system ($c/a - 1 = 0.005$) as compared to the parent compound BaTiO_3 ($c/a - 1 = 0.01$) is consistent with this viewpoint. The appearance of metastable phases adds to the structural heterogeneity of the system, and appears to be beneficial for large piezoelectric response.

C. Significance of the identical stress- and electric-field-driven transformations

Before we end, we would like to comment on the similarity of the structural phase transformation induced by pressure and electric field. A similar equivalence of stress- and electric-field-driven transformation was shown for the MPB compositions of a soft PZT by Kalyani *et al.* [20] and PbTiO_3 - BiScO_3 by Lalitha *et al.* [21]. This feature appears to be a universal for all MPB piezoelectrics. At the outset, this observation may seem to imply that the structural state of a MPB piezoelectric represents a locked state of polarization and strain. By definition, the piezoelectric phenomenon is explained in terms of (i) direct piezoelectric effect- stress as the stimulus and polarization as the response, and (ii) converse piezoelectric effect in which electric field is the stimulus and strain is the response. As per phenomenological thermodynamic considerations, the piezoelectric coefficient (d) is expected to be the same irrespective of whether it is measured using the direct or the converse effect. Since the measured response of a piezoelectric is related to the mechanism(s), it may be suggested that in situations where structural transformation plays a dominant role in influencing the piezoelectric response, the similarity of the phase transformation induced by stress and electric field may have a relationship with similarity of the piezoresponse measured either by stress or electric field. It is, however, important to bear in mind that the invariance of the piezocoefficient is valid only in the linear (weak-field) regime, well below the coercive field. Our experiments, on the other hand, have been carried out at high electric-field and stress levels (300 MPa). Hence the suggested correlation between the invariance of the direct and converse piezocoefficient with the similarity of the phase transformation induced by stress and electric field should be taken tentatively. We may, however, note that similar to the motion of ferroelectric-ferroelastic domain walls, which are irreversible at large fields and reversible at weak fields [33],

we can expect the field/stress-driven transformation also to be reversible in the weak-field regime.

V. CONCLUSION

We have carried out a detailed study of the structural phase transformation behavior of the $0.5\text{Ba}(\text{Ti}_{0.8}\text{Zr}_{0.2})\text{O}_3 - 0.5(\text{Ba}_{0.7}\text{Ca}_{0.3})\text{TiO}_3$ as a function of temperature, stress, and electric field. The system exhibits orthorhombic and rhombohedral structures as metastable phases in a wide range of temperature. Our study also suggests that the large piezoelectric response near room temperature has a notable contribution from increased fraction of the metastable

orthorhombic phase after poling. Using a “powder-poling” technique we demonstrate that the nature of the structural transformation ($P4mm \rightarrow Amm2 + R3m$) is the same irrespective of whether the stress or electric field is applied on the specimen.

ACKNOWLEDGMENTS

K.B. gratefully acknowledges the National Post Doctoral Fellowship (NPDF) of the Science and Engineering Research Board (SERB), Department of Science and Technology, Government of India. R.R. acknowledges SERB (Grant No. SERB/F/5046/2013-14) and ISRO-IISc, Space Technology Cell, for financial assistance.

-
- [1] W. Liu and X. Ren, *Phys. Rev. Lett.* **103**, 257602 (2009).
- [2] D. Damjanovic, A. Biancoli, L. Batooli, A. Vahabzadeh, and J. Trodahl, *Appl. Phys. Lett.* **100**, 192907 (2012).
- [3] A. B. Haugen, J. S. Forrester, D. Damjanovic, B. Li, K. J. Bowman, and J. L. Jones, *J. Appl. Phys.* **113**, 014103 (2013).
- [4] D. S. Keeble, F. Benabdallah, P. A. Thomas, M. Maglione, and J. Kreisel, *Appl. Phys. Lett.* **102**, 092903 (2013).
- [5] J. Gao, L. Zhang, D. Xue, T. Kimoto, M. Song, L. Zhong, and X. Ren, *J. Appl. Phys.* **115**, 054108 (2014).
- [6] M. Acosta, N. Khakpash, T. Someya, N. Novak, W. Jo, H. Nagata, G. A. Rossetti, Jr., and J. Rödel, *Phys. Rev. B* **91**, 104108 (2015).
- [7] K. Brajesh, K. Tanwar, M. Abebe, and R. Ranjan, *Phys. Rev. B* **92**, 224112 (2015).
- [8] M. Acosta, N. Novak, W. Jo, and J. Roedel, *Acta Mater.* **80**, 48 (2014).
- [9] A. K. Kalyani, H. Krishnan, A. Sen, A. Senyshyn, and R. Ranjan, *Phys. Rev. B* **91**, 024101 (2015).
- [10] A. K. Kalyani, A. Senyshyn, and R. Ranjan, *J. Appl. Phys.* **114**, 014102 (2013).
- [11] A. K. Kalyani, K. Brajesh, A. Senyshyn, and R. Ranjan, *Appl. Phys. Lett.* **104**, 252906 (2014).
- [12] J. Gao, D. Xue, Y. Wang, L. Zhang, H. Wu, S. Guo, H. Bao, C. Zhou, W. Liu, S. Hou, G. Xiao, and X. Ren, *Appl. Phys. Lett.* **99**, 092901 (2011).
- [13] L. Zhang, M. Zhang, L. Wang, C. Zhou, Z. Zhang, Y. Yao, L. Zhang, D. Xue, X. Lou, and X. Ren, *Appl. Phys. Lett.* **105**, 162908 (2014).
- [14] Y. Tian, X. Chao, L. Jin, L. Wei, P. Lianag, and Z. Yang, *Appl. Phys. Lett.* **104**, 112901 (2014).
- [15] G. Tutuncu, B. Li, K. Bowman, and J. L. Jones, *J. Appl. Phys.* **115**, 144104 (2014).
- [16] M. C. Ehmke, N. H. Khansur, J. E. Daniels, J. E. Blendell, and K. J. Bowman, *Acta Mater.* **66**, 340 (2014).
- [17] M. Hinterstein, M. Hoelzel, J. Rouquette, J. Haines, J. Glaum, H. Kungl, and M. Hoffman, *Acta Mater.* **94**, 319 (2015).
- [18] D. K. Khatua, Lalitha K. V., C. M. Fancher, J. L. Jones, and R. Ranjan, *Phys. Rev. B* **93**, 104103 (2016).
- [19] Rodrigues-J. Carvajal, FULLPROF 2000, A Rietveld Refinement and Pattern Matching Analysis Program, Laboratories Leon Brillouin (CEA-CNRS), France, 2000.
- [20] A. K. Kalyani, Lalitha K. V., A. R. James, A. N. Fitch, and R. Ranjan, *J. Phys.: Condens. Matter* **27**, 072201 (2015).
- [21] Lalitha K. V., A. K. Kalyani, and R. Ranjan, *Phys. Rev. B* **90**, 224107 (2014).
- [22] A. K. Kalyani, D. K. Khatua, B. Loukya, R. Datta, A. N. Fitch, A. Senyshyn, and R. Ranjan, *Phys. Rev. B* **91**, 104104 (2015).
- [23] R. Garg, B. N. Rao, A. Senyshyn, and R. Ranjan, *J. Appl. Phys.* **114**, 234102 (2013).
- [24] D. K. Khatua, A. Senyshyn, and R. Ranjan, *Phys. Rev. B* **93**, 134106 (2016).
- [25] R. Garg, A. Senyshyn, and R. Ranjan, *J. Phys.: Condens. Matter* **24**, 455902 (2012).
- [26] G. A. Samara, *J. Phys.: Condens. Matter* **15**, R367 (2003).
- [27] A. R. Akbarzadeh, S. Prosandeev, E. J. Walter, A. Al-Barakaty, and L. Bellaiche, *Phys. Rev. Lett.* **108**, 257601 (2012).
- [28] S. Prosandeev, D. Wang, A. R. Akbarzadeh, and L. Bellaiche, *J. Phys.: Condens. Matter* **27**, 223202 (2015).
- [29] D. Wang, J. Hlinka, A. A. Bokov, Z.-G. Ye, P. Ondrejko, J. Petzelt, and L. Bellaiche, *Nat. Commun.* **5**, 5100 (2014).
- [30] J. Petzelt, D. Nuzhnyy, V. Bovtun, M. Kempa, M. Savinov, S. Kamba, and J. Hlinka, *Phase Trans.* **88**, 320 (2015).
- [31] J. Petzelt, D. Nuzhnyy, M. Savinov, V. Bovtun, M. Kempa, T. Ostapchuk, J. Hlinka, G. Canu, and V. Buscaglia, *Ferroelectrics* **469**, 14 (2014).
- [32] D. Nuzhnyy, J. Petzelt, M. Savinov, T. Ostapchuk, V. Bovtun, M. Kempa, J. Hlinka, V. Buscaglia, M. T. Buscaglia, and P. Nanni, *Phys. Rev. B* **86**, 014106 (2012).
- [33] D. Damjanovic, *Rep. Prog. Phys.* **61**, 1267 (1998).